ACADEMIC PRESS

Available online at www.sciencedirect.com
SCIENCE DIRECT®

Journal of Catalysis 214 (2003) 33–45

JOURNAL OF CATALYSIS

www.elsevier.com/locate/jcat

Steam-activated FeMFI zeolites. Evolution of iron species and activity in direct N_2O decomposition

J. Pérez-Ramírez,[a,*] F. Kapteijn,[b] J.C. Groen,[c] A. Doménech,[d] G. Mul,[b] and J.A. Moulijn [b]

[a] *Hydrocarbon Processes and Catalysis, Oil & Energy Research Centre, Norsk Hydro, PO Box 2560, N-3907, Porsgrunn, Norway*
[b] *Reactor & Catalysis Engineering, DelftChemTech, Delft University of Technology, Julianalaan 136, 2628 BL, Delft, The Netherlands*
[c] *Applied Catalyst Characterization, DelftChemTech, Delft University of Technology, Julianalaan 136, 2628 BL, Delft, The Netherlands*
[d] *Department of Analytical Chemistry, University of Valencia, Dr. Moliner 50, 46100, Burjassot, Valencia, Spain*

Received 10 May 2002; revised 7 August 2002; accepted 16 September 2002

Abstract

In this paper the effect of the composition and steaming conditions of FeMFI catalysts on activity in direct N_2O decomposition is investigated. MFI zeolites with different framework compositions (Fe–Al–Si, Fe–Ga–Si, and Fe–Si) and without iron (< 0.002 wt% Fe in the final catalyst) were activated at different temperatures (673–1273 K) and partial steam pressures (20–500 mbar). Extra-framework Fe is essential for high catalytic activity in direct N_2O decomposition, while Lewis and Brønsted acidic sites play a minor role. Optimized activity was obtained at lower activation temperatures for the iron zeolites containing Al and Ga (873–923 K) than in the purely siliceous zeolite catalyst (1123 K), indicating relatively high stability of Fe in the silicalite framework. High partial steam pressures (> 100 mbar H_2O in N_2) favor the extraction of framework iron, enabling the application of lower activation temperatures. The optimum temperature during steam activation is that at which extraction of framework iron is complete without extensive clustering of extra-framework iron species into oxide particles, as was demonstrated by transmission electron microscopy and electrochemical characterization of the samples. Additional experiments showed an increase in activity as a function of decreasing crystal size of the zeolite, indicating the presence of intracrystalline transport limitations. Furthermore, higher N_2O decomposition activities can be obtained by the application of a novel alkaline post-treatment of the steamed catalyst to further improve the catalyst accessibility by creation of mesopores. Implications of the results for the nature of the active Fe-site in direct N_2O decomposition are discussed. Our observations suggest that small intrazeolitic iron species in extra-framework positions are crucial in direct N_2O decomposition.

Keywords: N_2O decomposition; FeMFI; Iron species; Active sites; Extra-framework; Activation; Steam treatment; Alkaline treatment; Diffusion limitations; Voltammetric response

1. Introduction

Steam treatment of isomorphously substituted FeZSM-5 zeolites has led to catalysts with outstanding properties in various processes. Steam-treated FeMFI has been found beneficial in the selective oxidation of benzene to phenol with N_2O [1–5], where it not only induces a higher phenol productivity and lower activity decay than for thermal activation in vacuum, but also leads to a much lower activation temperature (873–898 K in steam vs 1173 K in vacuum) [1]. We have also shown the excellent performance (activity and stability) of steamed FeZSM-5 compared to FeZSM-5 catalysts prepared by other methods in the direct decomposition of N_2O in simulated tail-gas from nitric acid plants and combustion processes [6,7].

Upon steam treatment, tetrahedral iron is extracted from tetrahedral framework positions by hydrolysis of Si–O–Fe bonds. The formation of extra-framework iron species induced by calcination and steam treatment of FeZSM-5 (in 30 vol% H_2O at 873 K for 5 h) has been described elsewhere [8]. This complex process can be envisaged as a clustering process, leading to various iron species in the final catalyst, including isolated iron and oligonuclear iron species, as well as highly dispersed iron oxide nanoparticles of 1–2 nm. Steam treatment also induces extensive dealumination of the zeolite and decreased density of Brønsted acidic sites. The iron species in steamed FeMFI samples

* Corresponding author.
E-mail address: javier.perez.ramirez@hydro.com (J. Pérez-Ramírez).

0021-9517/03/$ – see front matter
doi:10.1016/S0021-9517(02)00021-0

with various framework compositions and iron contents have also been discussed elsewhere [5,9,10]. However, to the best of our knowledge, a systematic analysis of the activation conditions (temperature and partial steam pressure) has not been reported. This should lead to an optimized catalyst and improved understanding of the evolution of Fe upon extraction from the zeolite framework.

In this paper, we discuss the nature of various species in steamed FeMFI zeolites at different activation conditions and their role for direct N_2O decomposition. To this end, zeolite catalysts with different framework compositions (Fe–Al–Si, Fe–Ga–Si, and Fe–Si) and without iron in the synthesis gel (< 0.002 wt%) have been synthesized and activated in steam at different temperatures (673–1273 K) and partial steam pressures (20–500 mbar). The samples have been characterized by a combination of conventional (ICP-OES, neutron activation analysis, XRD, SEM, ^{27}Al and ^{71}Ga MAS–NMR, N_2 adsorption, TEM) and nontraditional (voltammetric response) techniques. Electrochemical characterization was used to identify the nature of the Fe species in the various samples. Furthermore, variation of the crystal size by using different concentrations of template during zeolite synthesis and post-synthesis modification of the pore structure of the zeolite matrix by alkaline treatment were investigated to evaluate the location of the active Fe species in the direct catalytic decomposition of N_2O.

2. Experimental

2.1. Catalyst preparation

2.1.1. Hydrothermal synthesis

Isomorphously substituted ferrialuminosilicate [Fe,Al]MFI, ferrigallosilicate [Fe,Ga]MFI, and ferrisilicate [Fe]MFI and the same zeolites without iron, i.e., [Al]MFI, [Ga]MFI, and [–]MFI (silicalite-1), were synthesized hydrothermally using TPAOH as the template [2,8]. High-purity chemicals were used in the preparations ($> 99.995\%$) to avoid any contamination of the samples by iron. The nominal molar ratio between the components was $H_2O/Si = 45$, $TPAOH/Si = 0.1$, $NaOH/Si = 0.2$, Si/Al or $Si/Ga = 36$, and $Si/Fe = 152$. During the synthesis, a solution of the silica source (TEOS), and NaOH was added to a mixture of the metal nitrates. The solution was transferred to a stainless steel autoclave lined with Teflon and kept in a static air oven at 448 K for 5 days. The crystalline material was filtered and washed with deionized water until the sample was free of nitrates.

In a modified synthesis, [Fe,Al]MFI was prepared by excluding NaOH in the synthesis gel and increasing the concentration of TPAOH. In this case, $NaOH/Si$ and $TPAOH/Si$ were 0 and 0.3, respectively. The other molar ratios were kept constant. This sample is denoted as [Fe,Al]MFI(*sc*), where *sc* stands for small crystal.

2.1.2. Calcination and steam treatment

The as-synthesized samples, containing the different metals in the zeolite framework, were calcined in air at 823 K for 10 h and converted into the H-form by three consecutive exchanges with an NH_4NO_3 solution (0.1 M) for 12 h and subsequent air calcination at 823 K for 5 h. Finally the catalysts were activated in a flow of nitrogen and steam at ambient pressure, using a water partial pressure of 20–500 mbar H_2O and 30 ml (STP) $\cdot$ min^{-1} of N_2 flow at seven different temperatures in the range 673–1273 K for 5 h. Along the manuscript, the calcined and steamed zeolites are denoted by the prefixes *c*- and *ex*-, respectively.

NH_4-ZSM-5 (CBV 8020, P&Q) was used as a reference material to determine the amount of iron in a commercial sample and evaluate its catalytic activity. The parent sample was calcined and steamed according to the procedure described above.

2.1.3. Alkaline post-treatment

The steamed ferrialuminosilicate was treated in alkaline solution according to the method described elsewhere [11]. Briefly, *ex*-[Fe,Al]MFI was stirred in a 0.2 M NaOH aqueous solution (pH = 13.3) at 353 K for 1 h. The slurry was then cooled down immediately using an ice bath, filtered, rinsed at 353 K with distilled water, and finally dried at 383 K. This sample is denoted as *ex*-[Fe,Al]MFI(*at*). The resulting filtrate was kept for analysis by ICP-OES.

2.2. Catalyst characterization

Chemical composition of the samples was determined by ICP-OES (Perkin–Elmer Plasma 40 (Si) and Optima 3000DV (axial)). For some samples, traces of iron were determined by instrumental neutron activation analysis.

Powder X-ray diffraction patterns were measured in a Bruker AXS diffractometer with Bragg–Brentano geometry and Cu-K_α radiation ($\lambda = 0.1541$ nm). Data were collected in the 2θ range of 5° to 50° at a scan rate of 0.5 ° min^{-1}.

Scanning electron microscopy images were recorded at 10 kV in a Philips XL 20 microscope. Samples were coated with gold to create contrast.

^{27}Al and ^{71}Ga magic angle spinning–nuclear magnetic resonance was recorded at 79.5 and 183.0 MHz, respectively, with a Varian VXR-400S spectrometer. The narrow bore magnet (50 mm) was fitted with a high-speed magic angle spinning (MAS) Doty probe. The samples were spun in 5-mm-diameter rotors made of zirconia. The length of the rf pulses was 0.5 μs for Al and 0.4 μs for Ga. The spinning frequency was 7.0 kHz for Al and 8.0 kHz for Ga. Acquisition time was 0.2 s for Al and 0.4 s for Ga. A time interval between successive accumulations of 1 s for Al and 3 s for Ga was selected in order to avoid saturation effects. The number of accumulations (10,000 for Al and 5000 for Ga) allowed a signal-to-noise ratio higher than 20. The ^{27}Al and ^{71}Ga chemical shifts were referenced to $Al(H_2O)_6^{3+}$ and $Ga(H_2O)_6^{3+}$, respectively.

N_2 adsorption at 77 K was carried out in a QuantaChrome Autosorb-6B apparatus. Samples were previously evacuated at 623 K for 16 h. The micropore volume (V_{micro}) and the macropore and mesopore surface area (S_t) were determined with the t-plot method according to Lippens and de Boer [12]. The BET method was used to calculate the total surface area (S_{BET}) of the samples, which is used for comparative purposes. The pore size distribution was derived from the adsorption branch of the isotherm by application of the BJH model [13].

Transmission electron microscopy was carried out on a Philips CM 30 T electron microscope with a LaB_6 filament as the source of electrons operated at 300 kV. In some cases, the zeolites were amorphized by the electron beam in order to enhance the visibility of the small iron oxide particles.

The voltammetric response of polyester–graphite composite electrodes (PGCEs) modified by FeMFI samples was measured in a standard three-electrode arrangement with a platinum auxiliary electrode and a saturated calomel reference electrode (SCE). A freshly polished glassy carbon electrode was used as working electrode. Preparation of the composite electrode and modification by the zeolite samples has been described elsewhere [8,14]. Polyester–graphite composite electrodes were prepared by adding 45 wt% graphite to 55 wt% polyester resin, freshly synthesized. Zeolite-modified electrodes were prepared by abrasive conditioning, placing 1–2 mg of the sample on a glazed porcelain tile forming a spot of finely distributed material. The lower end of the electrode was then pressed and vigorously rubbed against that spot of sample. Cathodic linear scan voltammograms (LSVs) were recorded at a potential scan rate (ν) of 20 $mV\,s^{-1}$ using a Metrohm E506 Polarecord. Experiments were performed at 298 K in aqueous solutions of 1.0 M HCl as supporting electrolyte under argon atmosphere.

2.3. Activity tests

Activity measurements were carried out in a six-flow reactor system [15], using 50 mg of catalyst (125–200 μm) and a space time of 8.65×10^5 $g\,s\,mol^{-1}$. The space time is defined as the ratio $W/F(N_2O)_o$, where W is the catalyst mass and $F(N_2O)_o$ the molar flow of N_2O at the reactor inlet. The feed composition was 1.5 mbar N_2O in He at atmospheric pressure. Before reaction, the catalysts were pretreated in the feed mixture at 723 K for 1 h and cooled in that gas flow to the initial reaction temperature. N_2O, N_2, and O_2 were analyzed with a GC (Chrompack CP 9001) equipped with a thermal conductivity detector, using a Poraplot Q column (for N_2O separation) and a Molsieve 5A column (for N_2 and O_2 separation).

Table 1
Chemical composition of the catalysts used

Catalyst	Si/(Al or Ga)	Fe/wt%
ex-[Al]MFI	32.5	< 0.002[a]
ex-[Ga]MFI	31.1	< 0.002[a]
ex-[–]MFI[b]	∞	< 0.002[a]
ex-[Fe,Al]MFI	31.3	0.67
ex-[Fe,Al]MFI(*sc*)	35.5	0.61
ex-[Fe,Ga]MFI	32.6	0.58
ex-[Fe]MFI	∞	0.68
ex-[Fe,Al]MFI(*at*)	26.3	0.78
ex-H-ZSM-5[c]	37.5	0.017[a]

[a] Instrumental neutron activation analysis.
[b] Silicalite-1.
[c] Commercial sample (steamed).

3. Results

3.1. Catalyst characterization

3.1.1. Chemical composition

Table 1 shows the chemical compositions of the different materials prepared in this study. The catalysts have comparable molar Si/(Al or Ga) ratios and iron content. The composition did not change with different steam treatments. The catalysts prepared by excluding iron show Fe levels < 0.002 wt% (detection limit of the neutron activation analysis). The commercial steamed H-ZSM-5 contained 170 ppmw of iron. The chemical composition of the steamed Fe–Al zeolite and the product obtained after NaOH treatment, *ex*-[Fe,Al]MFI(*at*), is significantly different. The molar Si/Al ratio of the last sample is reduced by ∼ 20% as a consequence of extensive Si leaching in alkaline medium. This was confirmed by the analysis of the filtrate. The filtrate contained a negligible amount of Al and Fe. The preferential removal of silicon in the alkaline-treated catalysts results in a higher iron (and aluminum) content per gram of catalyst (see Table 1). The mass balances for the different components (Si, Al, Fe, and O) were within 1–2% and indicated that silicon is removed as SiO_2.

3.1.2. XRD and SEM

The X-ray diffraction patterns of the as-synthesized zeolites correspond to materials with the MFI structure. The long-range crystalline order and the crystal size of the as-synthesized zeolites was not altered by the different post-synthesis treatments (calcination, steaming under different conditions, and alkaline treatment), as concluded from XRD and SEM analyses. This was already shown for [Fe,Al]MFI [2,8] and is also applicable to the [Fe,Ga]MFI and [Fe]MFI systems. The zeolites prepared using TPAOH/Si = 0.2 and NaOH/Si = 0.1 show a uniform crystal size distribution (ranging from 2.0 to 2.5 μm in size). The zeolite prepared with a higher template concentration (TPAOH/Si = 0.3 and no NaOH), yielding *ex*-[Fe,Al]MFI(*sc*), has shown a significantly (∼ 5–6 times) smaller crystal size (∼ 0.4 μm) [2]. The hydrophobic character of the alkyl chains of tetraalky-

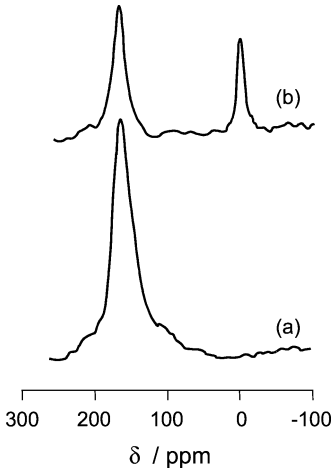

Fig. 1. ^{71}Ga MAS–NMR spectra of (a) *c*-[Fe,Ga]MFI and (b) *ex*-[Fe, Ga]MFI.

lammonium cations (TPA^+) favors the nucleation of zeolite crystals due to their templating or structure-directing properties, thus promoting the formation of many smaller crystals [16,17].

3.1.3. MAS–NMR

The ^{71}Ga MAS–NMR spectrum of *c*-[Fe,Ga]MFI shows one resonance at 160 ppm, which has been assigned to tetrahedrally coordinated Ga in lattice positions (Fig. 1) [18]. The broad signal is due to the high quadrupolar interactions of the gallium nuclei. Steam treatment leads to dislodgment of Ga(III) species of the zeolite to extra-framework positions. In the spectrum of the steamed sample (in 300 mbar H_2O at 873 K for 5 h) the resonance around 160 ppm significantly decreases and a band centered at 0 ppm appears. This band is typical of octahedrally coordinated gallium species [19].

Steam treatment also leads to dealumination of the zeolite sample containing Al, as reported elsewhere [8]. The calcined zeolite showed a relatively sharp response at 55 ppm, attributed to tetrahedrally coordinated Al in the zeolite framework, while in the steamed zeolite this resonance significantly decreased and a broad band centered at −3 ppm appeared, with a shoulder at 30 ppm. The peak at −3 ppm was attributed to hexacoordinated Al species in octahedral positions, while the shoulder at 30 ppm indicated pentacoordinated Al species in nonframework positions.

3.1.4. N_2 adsorption

Activation by steam. Table 2 shows the adsorption parameters of the calcined and steamed zeolites, as obtained from the N_2 adsorption isotherms in Fig. 2. The total pore volumes of the samples are similar. A slight decrease in the micropore volume, coupled to an increase of the mesopore surface area and a decrease of the BET surface area, is identified upon steam treatment of the Al- and Ga-containing zeolites. This suggests that a small fraction of micropores are converted to mesopores due to the extraction of Al and Ga to extra-framework positions upon steam treatment. This can also be concluded from the hysteresis in the adsorption–desorption isotherms at $p/p_0 > 0.45$ (Figs. 2b, 2c), which is absent in the calcined-only material (Fig. 2a). The isotherm of *ex*-[Fe]MFI resembles that of the calcined precursor (compare Figs. 2a and 2d), indicating a similar texture before and after steam treatment. This result suggests a higher stability of ferrisilicalite against steam treatment and that the textural changes in the other zeolites are mainly caused by the presence of extractable Al and Ga framework species. The same trend was observed in the zeolite samples containing no iron. The textural properties of the large and small crystal *ex*-[Fe,Al]MFI zeolites are also very similar, the latter showing a slightly larger S_t surface area, which can be ascribed to the higher external surface area of the smaller crystals.

Table 2
Textural properties of the calcined and steamed FeMFI catalysts

Catalyst	V_{micro} ($cm^3\,g^{-1}$)[a]	V_{total} ($m^3\,g^{-1}$)	S_t ($cm^2\,g^{-1}$)[a]	S_{BET} ($m^2\,g^{-1}$)[b]
c-[Fe,Al]MFI	0.16	0.24	22	425
ex-[Fe,Al]MFI	0.14	0.23	32	372
ex-[Fe,Al]MFI(*sc*)	0.14	0.23	44	380
ex-[Fe,Al]MFI(*at*)	0.11	0.57	140	415
c-[Fe,Ga]MFI	0.16	0.25	39	423
ex-[Fe,Ga]MFI	0.15	0.24	51	385
c-[Fe]MFI	0.18	0.23	17	427
ex-[Fe]MFI	0.18	0.23	22	431

[a] t-plot method.
[b] BET method.

Alkaline post-treatment. Alkaline treatment of *ex*-[Fe, Al]MFI leads to substantial changes in the N_2 adsorption isotherms. The type I isotherm in *ex*-[Fe,Al]MFI, with a plateau at high p/p_0 (Fig. 3a), which is characteristic of microporous materials without significant meso- or macroporosity, contrasts with the behavior of the alkaline-treated sample (Fig. 3b). *Ex*-FeZSM-5(*at*) shows a much higher adsorption capacity at $p/p_0 > 0.4$ as a result of newly created mesoporosity around 10 nm (inset in Fig. 3). The apparent difference between the isotherms of *ex*-[Fe,Al]MFI in Figs. 2b and 3a is due to the different scale. The progressive increase at $p/p_0 \sim 1$ in the alkaline-treated sample is probably a result of the enhanced surface roughness of the crystals as a result of the alkaline treatment, as was identified by SEM analysis [20,21]. Table 2 shows that some destruction of micropores ($\sim 0.05\ cm^3\,g^{-1}$) and considerable mesopore formation ($\sim 0.4\ cm^3\,g^{-1}$ and $140\ m^2\,g^{-1}$) take place by the alkaline treatment.

3.1.5. TEM

Activation by steam. The TEM micrographs of the steamed [Fe,Al]MFI and [Fe,Ga]MFI samples activated in 300 mbar H_2O in N_2 at 873 K for 5 h show the formation of homogeneous nanoparticles 1–2 nm in size (Figs. 4a, 4b), which are likely situated at the external surface of the zeolite crystal (extrazeolitic species). These nanoparticles

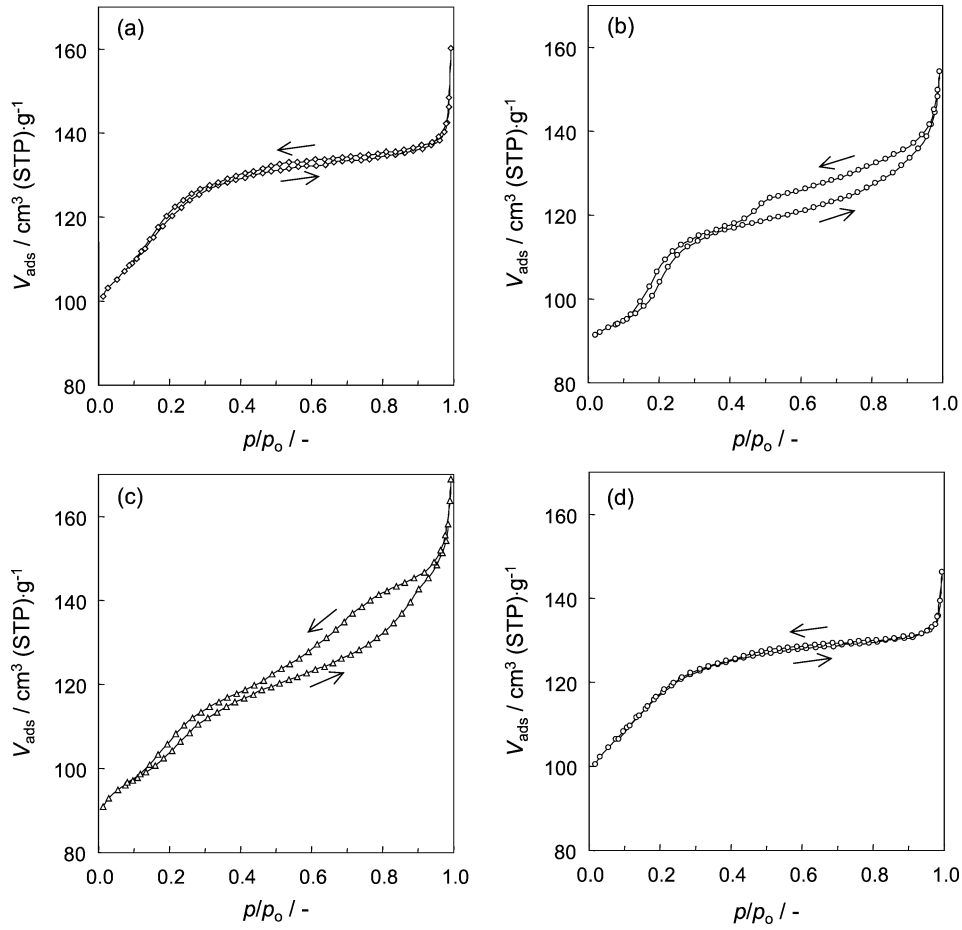

Fig. 2. N_2 adsorption–desorption isotherms at 77 K of (a) *c*-[Fe,Al]MFI, (b) *ex*-[Fe,Al]MFI, (c) *ex*-[Fe,Ga]MFI, and (d) *ex*-[Fe]MFI. Conditions of steam treatment: 300 mbar H_2O in N_2 at 873 K for 5 h.

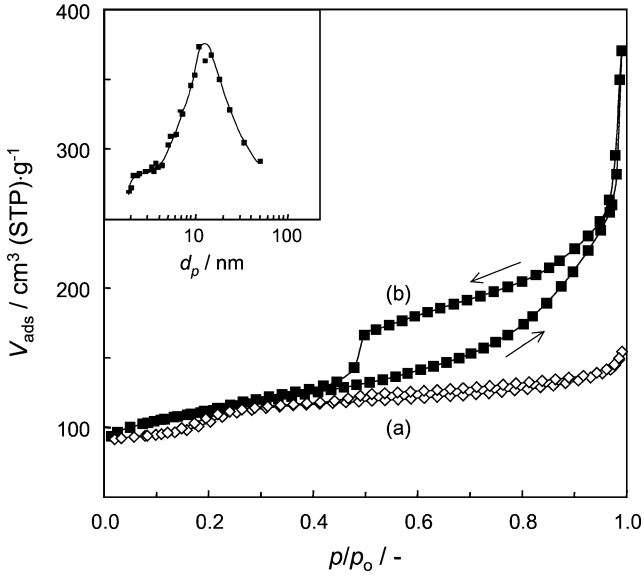

Fig. 3. N_2 adsorption–desorption isotherms at 77 K of (a) *ex*-[Fe,Al]MFI and (b) *ex*-[Fe,Al]MFI(*at*). Inset figure: pore size distribution determined from the adsorption branch of the isotherm of *ex*-[Fe,Al]MFI(*at*), using the BJH model [13].

were not observed in TEM micrographs of the analogous steamed sample without iron, *ex*-[Al]MFI or *ex*-[Ga]MFI, i.e., containing extra-framework Al and Ga species, suggesting that they mainly contain iron oxide. However, due to the massive extraction of Al and Ga upon steam treatment as indicated by MAS–NMR, the presence of Al or Ga in these particles cannot be excluded. After steaming at 873 K these nanoparticles were not observed in *ex*-[Fe]MFI (Fig. 4c), suggesting that a large fraction of iron in the sample is still in tetrahedral (framework) positions. Indeed, after steaming at 1123 K nanoparticles of similar size to those in *ex*-[Fe,Al]MFI and *ex*-[Fe,Ga]MFI (Figs. 4a, 4b) were observed. The particle size distribution of iron oxide is slightly smaller than in the samples containing Al and Ga steamed at 1123 K, indicating somewhat less clustering of iron.

Alkaline post-treatment. Fig. 5 shows the TEM micrographs of *ex*-[Fe,Al]MFI before and after the alkaline treatment. The steamed sample (Fig. 5a) shows the lattice planes of the zeolite. Iron oxide particles can be observed, being more clearly visible in the high-magnification micrograph (Fig. 4a). Upon alkaline treatment, the lattice planes of the

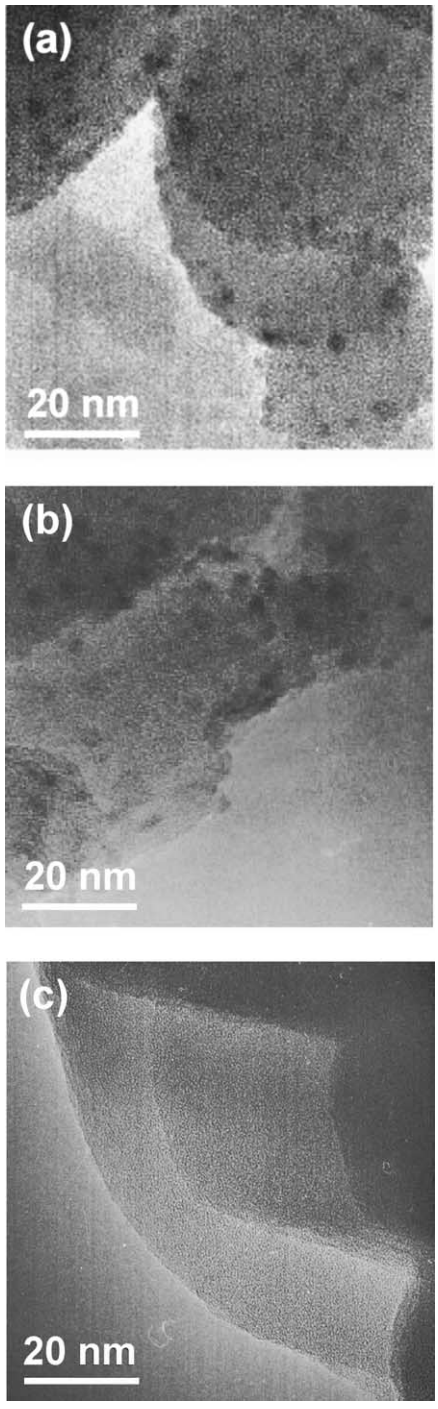

Fig. 4. High-resolution TEM micrographs of (a) *ex*-[Fe,Al]MFI, (b) *ex*-[Fe, Ga]MFI, and (c) *ex*-[Fe]MFI. Steam treatment: 300 mbar H_2O in N_2 at 873 K for 5 h.

zeolite can be still observed, in agreement with XRD, but an extensive number of mesopores are formed (Fig. 5b). The size of the "holes" observed in the zeolite crystal can be estimated to be around 10 nm, in good agreement with the pore size distribution of this sample as derived from N_2 adsorption (see inset in Fig. 3). A second change occurring upon alkaline treatment of the zeolite is that the iron oxide nanoparticles observed in the steamed material are now invisible. This has been ensured by taking high-magnification pictures of this sample, which only showed the zeolite crystal.

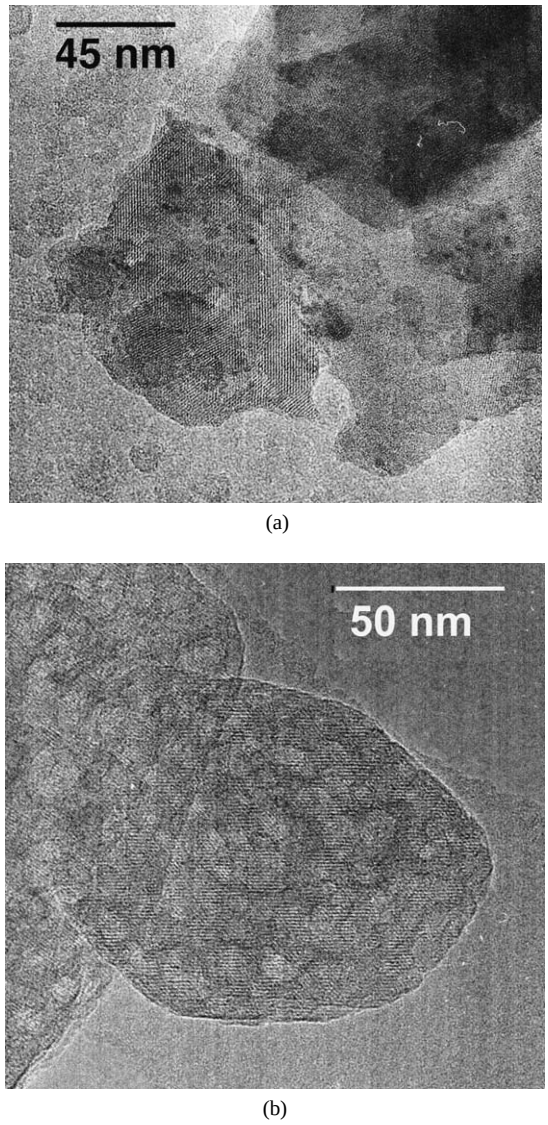

Fig. 5. TEM micrographs of (a) *ex*-[Fe,Al]MFI and (b) *ex*-[Fe,Al]MFI(*at*).

3.1.6. Voltammetric response

Activation by steam. The voltammetric response of graphite–polyester electrodes modified with the zeolite samples provides useful information on the evolution of the iron species in the catalysts. This novel solid-state electrochemical technique has been successfully applied to discriminate the various iron species during calcination and steam treatment of isomorphously substituted FeZSM-5 [8,14,22]. A limitation of the method is that quantification of the relative fractions of iron species is not possible, due to the intrinsic electron transfer mechanism of the electrochemical process [22].

The cathodic voltammetric responses C_1–C_7 shown in Fig. 6 have been assigned in detail elsewhere [14,22].

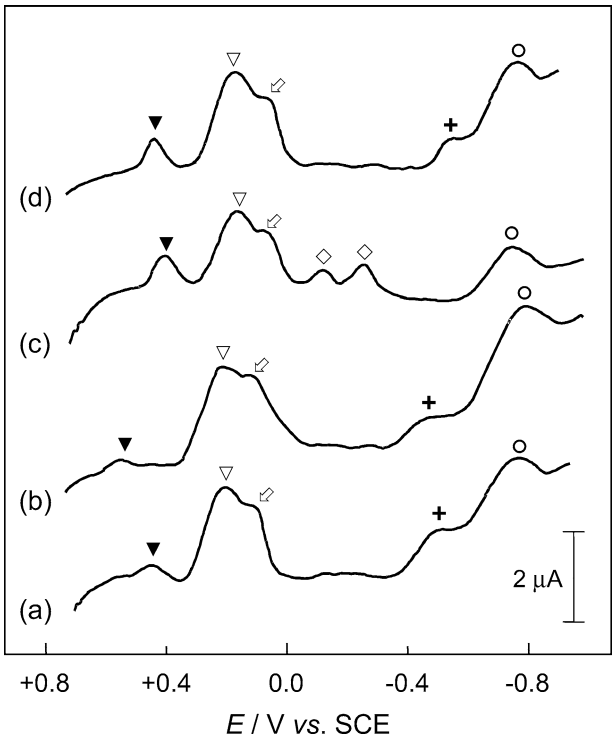

Symbol	Name	Assignement	Electrochemical process
▼	C_1	Oligonuclear Fe-ions	Electron-transfer (species in the solid)
▽	C_2	Isolated Fe-ions	Electron-transfer (species in the solid)
⬀	C_3	$Fe^{3+} \rightarrow Fe^{2+}$	Electron-transfer (species in dissolution)
◇	C_4, C_5	Framework Fe-ions	Electron-transfer (species in the solid)
+	C_6	Fe-oxide	Reductive dissolution
○	C_7	$Fe^{2+} \rightarrow Fe^0$	Metal deposition

Fig. 6. Linear scanning voltammetry responses in 1.0 M HCl aqueous solution of GCEs electrodes modified by (a) *ex*-[Fe,Al]MFI (873 K), (b) *ex*-[Fe,Ga]MFI (873 K), (c) *ex*-[Fe]MFI (873 K), (d) *ex*-[Fe]MFI (1123 K); $\nu = 20$ mV s^{-1}. Steam activation temperatures between brackets (see Refs. [27] and [38] for a detailed assignment).

A summary of these assignments is shown in the same figure and is briefly described below. The process C_6 (+) in *ex*-[Fe,Al]MFI and *ex*-[Fe,Ga]MFI (Figs. 6a, 6b), which were activated in 300 mbar H_2O in N_2 at 873 K for 5 h, is attributed to the reductive dissolution of iron oxide nanoparticles (observed by TEM) to Fe^{2+} in solution. This response is not present in *ex*-[Fe]MFI under these activation conditions (Fig. 6c), which is in good agreement with TEM analysis (see Fig. 4c) and in situ IR spectra of adsorbed NO [23]. Processes C_1 (▽) and C_2 (▼) have been assigned to oligonuclear oxo–iron species and isolated iron ions in extra-framework positions, respectively, and are present in all samples. The peak potential of the process C_1 in *ex*-[Fe,Ga]MFI is shifted to more positive potentials, which suggests an easier reducibility of the species in this zeolite. *Ex*-[Fe]MFI shows two well-defined peaks C_4 and C_5 (◇ in Fig. 6c), which indicate the presence of a substantial amount of iron in tetrahedral coordination. These peaks are virtually absent in *ex*-[Fe,Al]MFI and *ex*-[Fe,Ga]MFI. This result confirms the more difficult dislodgement of framework iron ions in Fe-silicalite compared to those additionally containing Al or Ga. Peaks C_3 (⬀) and C_7 (○) are assigned to the reduction of electrochemically generated Fe^{3+} (to Fe^{2+}) and Fe^{2+} (to Fe^0) in solution [14].

Effective extraction of isomorphously substituted iron ions in *ex*-[Fe]MFI can be achieved by performing the steam activation at a higher temperature (1123 K), as concluded by the decreased intensity of the C_4 and C_5 signals (◇). This severe treatment leads to clustering of extra-framework iron species into iron oxide nanoparticles (peak C_6, +, in Fig. 6d). This is in good agreement with TEM, since nanoparticles were identified at this activation temperature. The [Fe,Al]MFI and [Fe,Ga]MFI zeolites steamed at 1123 K lead to the following result: the intensity of the signal corresponding to iron oxide increases (C_6, +), coupled with decreased intensity of the peaks belonging to iron species in isolated positions (C_2, ▽) or in small oligonuclear intrazeolitic complexes (C_1, ▼). This result suggests the presence of a larger relative amount of iron oxide in the samples treated at higher temperatures, due to the clustering of small iron species during steam treatment at higher temperature. This was also suggested from TEM analysis. There is thus a strong dependency of the constitution of the catalyst, i.e., the nature and relative amount of iron species, on the framework composition and the conditions of steam activation.

Alkaline post-treatment. The NaOH-treated *ex*-[Fe,Al]MFI(*at*) shows a response very similar to that of its precursor, i.e., the steamed catalyst in Fig. 6a, indicating that the nature and distribution of the iron species are not altered by this post-treatment.

3.2. Activity

3.2.1. Importance of the steam activation

Fig. 7 shows the N_2O conversion vs temperature curves of isomorphously substituted FeMFI after calcination (at 823 K for 5 h) and steam treatment (in 300 mbar H_2O in N_2 at 873 K for 5 h). Activation of the zeolites with steam is crucial to create active species in the catalysts. The steamed catalysts show significant conversion at 700 K, while the calcined samples only exhibit measurable conversion at 800 K. The steamed catalysts containing Al and Ga give almost identical conversions, higher than *ex*-[Fe]MFI. The calcined catalysts yield a very similar (low) conversion independently of the framework composition. Apparently, iron ions of tetrahedral coordination in the zeolite framework, mainly present in the calcined zeolites, play no role in this reaction. Activation of N_2O, the first step in direct decomposition as well as in other N_2O-related conversions, requires

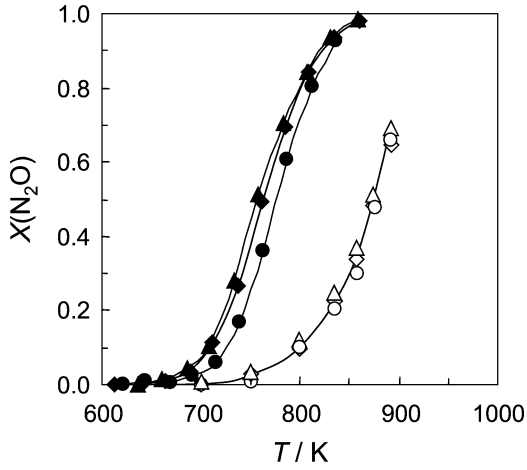

Fig. 7. N_2O conversion vs temperature over (▲) *ex*-[Fe,Al]MFI, (◆) *ex*-[Fe,Ga]MFI, (●) *ex*-[Fe]MFI, (△) *c*-[Fe,Al]MFI, (◇) *c*-[Fe, Ga]MFI, and (○) *c*-[Fe]MFI. Conditions: 1.5 mbar N_2O in He, $W/F(N_2O)_o = 8.65 \times 10^5$ g s mol^{-1}, $P = 1$ bar.

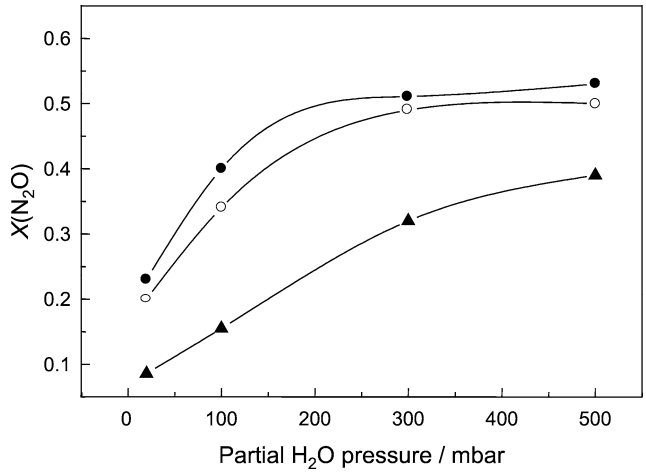

Fig. 8. N_2O conversion at 748 K vs partial H_2O pressure during steam treatment at 873 K for 5 h over (●) *ex*-[Fe,Al]MFI, (○) *ex*-[Fe, Ga]MFI, and (▲) *ex*-[Fe]MFI. Reaction conditions: 1.5 mbar N_2O in He, $W/F(N_2O)_o = 8.65 \times 10^5$ g s mol^{-1}, $P = 1$ bar.

coordination of atomic oxygen to the active site, which is impossible for framework iron.

3.2.2. Optimization of the steam treatment

The catalyst constitution with respect to iron is the most important factor explaining the activity curves of the steamed catalysts shown in Fig. 7. A significant fraction of iron in (inactive) framework positions was identified in the voltammetric response of *ex*-[Fe]MFI, which in principle accounts for the lower activity compared to the catalysts containing Al and Ga, where the extraction of framework iron was more extensive. This result suggests that there exists an optimal activation treatment for maximizing the N_2O decomposition activity. Therefore, the N_2O decomposition activity was measured for FeMFI catalysts activated at different conditions of partial steam pressures (20–500 mbar H_2O in N_2) and temperatures (673–1273 K) during 5 h.

Water content. Fig. 8 shows that the conversion of N_2O at 748 K increases with increasing H_2O pressure during steam treatment at 873 K. Significant improvement is observed in the range 0–300 mbar H_2O. At high steam contents, hydrolysis of Si–O–Fe bonds and thus dislodgement of framework iron to more active extra-framework positions is facilitated. Above 300 mbar H_2O there is little further improvement in N_2O conversion for the samples containing Al and Ga.

Activation temperature. The N_2O conversion over the steamed catalysts (at 300 mbar H_2O) measured at 748 K shows an optimal activation temperature (Fig. 9), which depends on the composition of the zeolite framework. *Ex*-[Fe,Al]MFI and *ex*-[Fe,Ga]MFI exhibit similar behavior, yielding the highest N_2O conversion at activation temperatures of 850–900 K. The position of this maximum is shifted to a significantly higher temperature in *ex*-[Fe]MFI, around

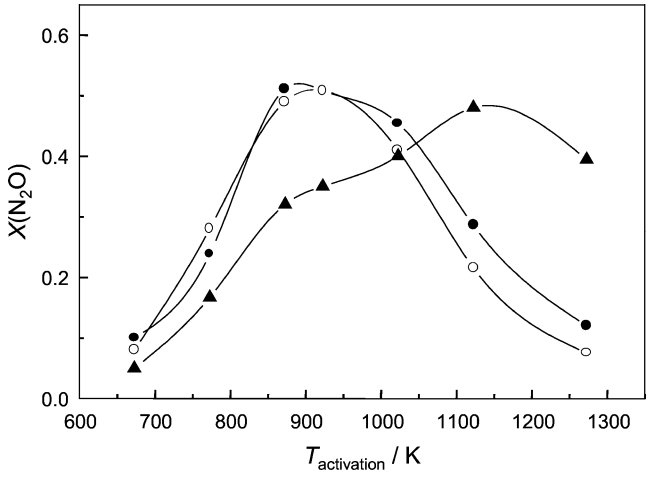

Fig. 9. N_2O conversion at 748 K vs activation temperature during steam treatment in 30 vol% H_2O for 5 h over (●) *ex*-[Fe,Al]MFI, (○) *ex*-[Fe,Ga]MFI, and (▲) *ex*-[Fe]MFI. Conditions: 1.5 mbar N_2O in He, $W/F(N_2O)_o = 8.65 \times 10^5$ g s mol^{-1}, $P = 1$ bar.

1125 K. The presence of an optimal temperature is explained as follows: below the optimum, a large fraction of iron is still in framework positions, i.e., unavailable for the N_2O decomposition reaction. The presence of Al or Ga destabilizes the zeolite framework, inducing easier escape of iron (at ~ 225 K lower activation temperature than in the siliceous catalyst). Above the optimal activation temperature, where the dislodgement of framework iron is complete, the activity drops as a consequence of the extensive clustering of intrazeolitic iron species migrating to the outer surface of the zeolite crystal to form iron oxide nanoparticles observed by TEM. The conversion over the three catalysts activated at the optimal temperature is fairly similar, proving that the activity differences in Fig. 7 are indeed a consequence of the suboptimal activation of *ex*-[Fe]MFI.

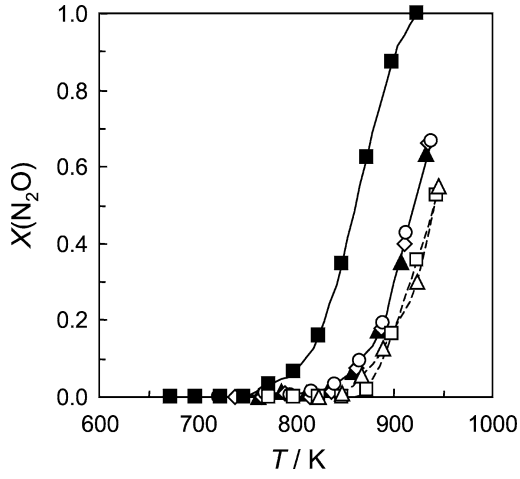

Fig. 10. N_2O conversion vs temperature over (▲) *ex*-[Al]MFI, (△) *c*-[Al]MFI, (◇) *ex*-[Ga]MFI, (○) *ex*-[–]MFI, (□) *c*-H-ZSM-5, and (■) *ex*-H-ZSM-5. Conditions: 1.5 mbar N_2O in He, $W/F(N_2O)_0 = 8.65 \times 10^5$ g s mol^{-1}, $P = 1$ bar.

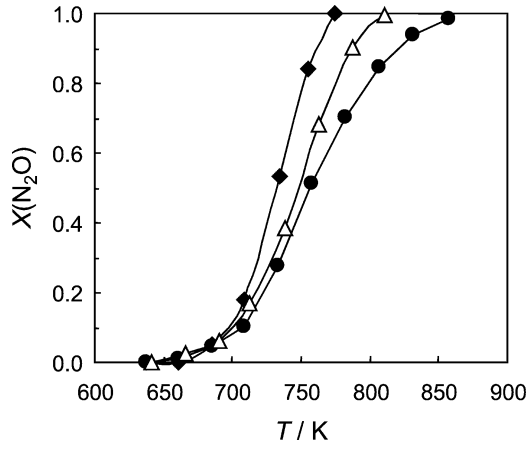

Fig. 11. N_2O conversion vs temperature over (●) *ex*-[Fe,Al]MFI, (△) *ex*-[Fe,Al]MFI(*sc*), and (◆) *ex*-[Fe,Al]MFI(*at*). Conditions: 1.5 mbar N_2O in He, $W/F(N_2O)_0 = 8.65 \times 10^5$ g s mol^{-1}, $P = 1$ bar.

3.2.3. Role of extra-framework Al and Ga species

The role of the generated Al and Ga extra-framework species under steam treatment was investigated by preparing the same zeolitic materials without Fe in the synthesis gel (< 20 ppmw Fe, see Table 1). Iron-free steam-activated catalysts, containing a significant amount of extra-framework Al and Ga species, exhibit much lower N_2O decomposition activities than the Fe-containing catalysts (compare Figs. 7 and 10). N_2O conversion was complete in *ex*-[Fe,X]MFI at 850 K, while no conversion was observed in *ex*-[X]MFI at this temperature. Furthermore, steam-treated purely siliceous zeolite (*ex*-[–]MFI) shows the same conversion as the steamed catalysts with Al or Ga (*ex*-[Al]MFI and *ex*-[Ga]MFI). Before and after steaming, the iron-free zeolites show nearly similar activities (see Fig. 10). These results indicate that the activation by steam in Fe-free zeolites does not improve direct N_2O decomposition and suggest a minor role of extra-framework Al and Ga species in the reaction.

Calcined commercial H-ZSM-5 shows activity similar to that of steam-activated zeolites prepared without iron. Significant improvement is obtained after steaming of the commercial zeolite, yielding *ex*-H-ZSM-5. This catalyst shows substantial N_2O conversion (36%) at 850 K, which, however, is still significantly lower than for the *ex*-[Fe]MFI catalysts. The increased N_2O decomposition activity is attributed to the presence of significant traces of iron (0.017 wt%, 170 ppmw) in the parent commercial zeolite. In the calcined commercial zeolite, iron is likely still present in framework positions, remaining inactive for N_2O decomposition. Only after steam treatment, the extraframework iron is active for the reaction.

3.2.4. Influence of the crystal size and alkaline treatment

Fig. 11 shows the activity curves of steamed Fe–Al–Si zeolites with different crystal sizes, as well as the sample post-treated in alkaline medium. For the samples of different crystal size, the N_2O decomposition activity is initiated at the same temperature (∼ 650 K), with similar conversion levels up to 715 K. Above this temperature the conversion over the zeolite with smaller crystal size (*ex*-[Fe,Al]MFI(*sc*) increases faster. Determination of the apparent activation energies from the slopes of the conversion–temperature curves (assuming first-order kinetics) leads to 137 and 161 kJ mol^{-1} for the catalysts with large (2.5 μm) and small crystals (0.4 μm), respectively. From the characteristic shapes of the activity curves (very similar activities at low temperature and lower apparent activation energy for the catalyst with large crystals), the activity differences can be explained by intracrystalline diffusion limitations.

Alkaline treatment of the catalyst with large crystals, *ex*-[Fe,Al]MFI(*at*), also leads to a significantly improved activity, going even beyond that of *ex*-[Fe,Al]MFI(*sc*). The apparent activation energy of the catalyst increases up to 185 kJ mol^{-1}. The slightly higher iron content in the alkaline-treated sample compared to the steamed sample does not fully account for the improved performance of *ex*-[Fe,Al]MFI(*at*) in N_2O decomposition (activity tests were performed with the same amount of catalyst (50 mg) at constant $W/F(N_2O)_0$). Calculation of the turnover frequency (TOF) of the different Fe–Al zeolites, i.e., the specific activity for N_2O decomposition per mol of (total) iron, indicates a significant relative improvement of activity. For example, at 730 K and under the conditions defined in the legend of Fig. 11, the turnover frequencies are calculated as 9 h^{-1} (*ex*-[Fe,Al]MFI), 12 h^{-1} (*ex*-[Fe,Al]MFI(*sc*)), and 15 h^{-1} (*ex*-[Fe,Al]MFI(*at*)).

4. Discussion

4.1. Relative activity of species in steamed FeMFI in direct N_2O decomposition

The experiments reported in this paper have shown that the presence of extraframework iron species, formed in

the steam treatment, is essential to obtain high activity of FeMFI catalysts in direct N_2O decomposition. Framework Fe species are saturated with oxygen of the zeolite lattice, being unable to coordinate atomic oxygen species (from N_2O). This is in agreement with the inability of isomorphously substituted iron in FeZSM-5 to activate N_2O for the selective oxidation of benzene to phenol [24,25].

The role of Brønsted acidic sites does not seem to be crucial for N_2O activation and decomposition, since steam treatment diminishes the concentration of strong acid sites appreciably [8], while the activity increases. Lewis acid sites are not relevant for N_2O decomposition either, since Fe-free MFI samples hardly show an improved N_2O conversion after steaming, whereas substantial amounts of extra-framework Al and Ga species are formed (see MAS–NMR). The sole presence of Al and Ga extra-framework species only induces activities above 850 K, much higher than the temperatures required for iron-containing catalysts (< 700 K). The role of these sites in selective oxidation of benzene to phenol with N_2O has been discussed elsewhere [26].

4.2. Tuning the catalyst constitution and performance. Optimal steam activation

Based on the characterization results shown here and elsewhere [23], the extraction of framework iron in FeMFI can be considered as a *clustering* process, leading to a redistribution of the iron species. This is schematically shown in Fig. 12. Dislodgement of framework iron to extra-framework positions takes place to form isolated ions in exchangeable positions, followed by clustering. Depending on the size of the thus formed oligonuclear cluster, this can be intrazeolitic, i.e., located in the zeolite channels ($(FeO)_n$, $n < 5$) [23,27], or extrazeolitic, i.e., located at the external surface of the zeolite crystal. A more severe treatment causes a more extensive degree of aggregation of iron entities into larger oligomers and ultimately results in the formation of iron oxide particles, like those visible in TEM (Figs. 4a, 4b).

The catalyst constitution, i.e., the nature and relative number of iron species in the catalysts, is greatly affected by the conditions of the steam treatment (partial steam pressure and temperature) and ultimately determines the activity of the formulation. The activation temperature should be

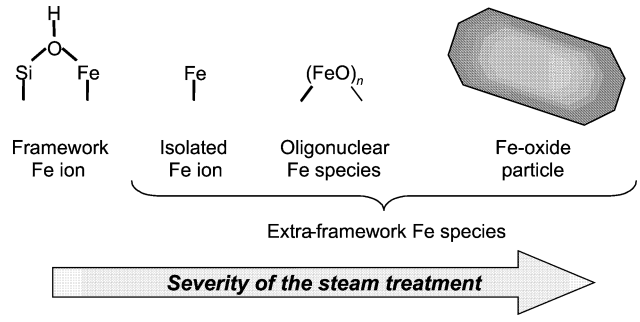

Fig. 12. Extraction and clustering of iron species in FeMFI catalysts upon steam activation.

adjusted to achieve the extraction of *inactive* framework iron but to avoid extensive clustering into *inactive* iron oxide particles. This is supported by the activity results in Fig. 7, where *ex*-[Fe]MFI, having no nanoparticles and still a significant fraction of iron in framework position, shows activity very similar to that of *ex*-[Fe,Al]MFI and *ex*-[Fe,Ga]MFI. From this, one can conclude that intrazeolitic iron species in extra-framework positions are essential to the reaction. However, achieving a state where 100% of the iron is in extraframework positions without any clustering into iron oxide appears to be very challenging, due to the heterogeneous distribution of iron species after the activation process.

Dislodgement of framework Fe is facilitated in the presence of Al or Ga, by destabilization of the zeolite framework, leading to lower optimal activation temperatures of 873–923 K (in 300 mbar H_2O for 5 h), compared to the higher temperature (1123 K) required for Fe-silicalite. The removal of Fe from framework positions was elegantly shown by electrochemical characterization. Unfortunately, no quantification of fraction of iron species is possible due to the intrinsic nature of the technique. Only a small fraction of electroactive species in the samples is being probed (estimated as 0.5 mol% of the total iron in the sample, $\sim$ 0.7 wt%), probably in the region of the zeolite grain in contact with the electrode surface [22]. This is due to the limited distance of electron tunneling. The surface-mediated electron-transfer mechanism is the most plausible description of this process, where the observed electrochemistry corresponds essentially to iron species in the "boundary" region of the zeolite [14,22].

After an optimum activation treatment, the N_2O decomposition activity is the same for all catalysts, but the milder treatment of the Al- and Ga-containing FeMFI zeolites makes their practical application more conceivable. The optimal steam activation temperature in our study of the Fe–Al–Si system for direct N_2O decomposition was very similar to that reported elsewhere for the benzene-to-phenol reaction [3].

The extent of extraction at certain activation conditions should be considered, otherwise it may lead to erroneous interpretations of activity data. Panov et al. [1,28,29] showed that the concentration of α-sites, which determines the catalyst activity in the benzene-to-phenol process, is 10–30 times lower in Fe–silicalite compared to FeZSM-5 for the same Fe content and activation conditions (1173 K in vacuum). In other words, 10–30 times more iron is needed in Fe-silicalite to have the same amount of α-oxygen. In a more recent publication by the same group, Fe-containing (Al–Si) and (Ga–Si) zeolite matrices have been compared with (B–Si) and (Ti–Si), leading to the conclusion that the neutral zeolites need 10–100 times more iron to achieve the same concentration of α-oxygen sites as in (Al–Si) and (Ga–Si) matrices [5]. This behavior has been attributed to the presence of charge-compensating cations in matrices with Brønsted acidity, which favors the mechanism of α-

site formation on iron sites as compared with neutral MFI matrices. Our results clearly indicate that due to the stability of framework iron in the siliceous matrix (and in general neutral zeolite matrices), a considerable amount of iron is still present as inactive framework iron after this treatment. Panov et al.'s results can be reinterpreted by stating that in the ZSM-5 matrix iron is dislodged to extra-framework positions 10–30 times more easily than in silicalite.

4.3. The role of intrapore diffusion in N_2O decomposition experiments

4.3.1. Effect of crystal size

The intrazeolitic nature of extra-framework iron species in FeMFI active for N_2O decomposition has been indicated by the activity results of *ex*-[Fe,Al]MFI of different crystal sizes (0.4 and 2.5 μm). Extensive characterization of both catalysts by EPR, TEM, FT-IR of NO adsorbed, H_2-TPR, UV–vis, and voltammetric response techniques according to the procedures described elsewhere [2,8,23] led to the conclusion that the iron species were of a similar nature. This in principle ruled out a different catalyst constitution to explain the different activities observed. The shape of the activity curves and apparent activation energies are attributed to the presence of diffusion transport limitations in the zeolite crystal. This result, which is the subject of the current research, can be attributed to both the relatively low diffusion coefficient of N_2O in the zeolite crystals (estimated to be $\sim 10^{-12}$ $m^2\,s^{-1}$, determing the Thiele modulus from the activity data) and the transport hindrance due to the presence of active species in the pores of the zeolite obstructing molecular transport. The presence of transport limitations might play a role in the various reactions catalyzed by FeMFI and should be considered as a general aspect to design improved catalysts. Intracrystalline diffusion limitations may also explain the higher activity of the zeolites with smaller crystals (*ex*-[Fe,Al]MFI(*sc*)) in the N_2O-mediated selective oxidation of benzene to phenol reported by some of us [2]. The presence of intracrystalline transport limitations over Co- and Cu-exchanged zeolites (Mor, Beta, MFI) has been identified for a similar process, the selective reduction of NO_x with light hydrocarbons [30,31], where zeolite crystals (0.2–1.3 μm) of size similar to that of those applied in this study were used. Tabata and Ohtsuka [30] estimated very low intracrystalline diffusion coefficients of NO in Co-ZSM-5 ($\sim 10^{-15}$ $m^2\,s^{-1}$), related to deNO_x SCR.

4.3.2. Effect of alkaline post-treatment

Post-treatment of the large crystal *ex*-[Fe,Al]MFI catalyst in NaOH at 353 K also leads to considerable improvement of the N_2O decomposition activity, even higher than observed for the zeolite with the small crystals (see Fig. 11). Associated with this improved activity, three observations concerning the post-treated material should be mentioned:

- Substantial leaching of silicon (as SiO_2) occurred, as was concluded from the analysis of the solid materials (steamed and alkaline-treated) and the corresponding filtrate. The amount of Fe and Al was not affected.
- Spectacular changes in the textural properties of the catalyst were identified: an extensive amount of mesopores was created, to the expense of a reduction of 30% of the micropore volume of the zeolite (Fig. 3 and Table 2).
- An "*apparent*" disappearance of iron oxide nanoparticles (compare Figs. 5a, 5b) was observed.

There is extensive knowledge of the acid treatment of zeolites to change the Si/Al in the framework, and thus the properties connected with this ratio [32]. Less information is available about the base treatment of zeolites. In contrast to the acid treatment, which preferentially removes framework Al atoms, the base treatment by the use of alkali solutions was found to preferentially remove framework siliceous species [33]. Previous studies on the alkaline treatment of MFI zeolites [34–37] by Na_2CO_3 or NaOH solutions showed that selective removal of the siliceous species occurs without changes in the crystallinity of the zeolite, in agreement with our XRD and TEM results. Application of TEM and N_2 adsorption indicates the generation of a broad size distribution of the mesopores, centered at 10 nm [11], and not uniformly distributed as claimed erroneously by Ogura et al. [38]. More harsh conditions (pH > 14) even result in macropore formation [20], visible by SEM. The selective dissolution of silicon appears to be responsible for the pore formation and thus a considerably reduced content of this metal in the post-treated solid is obtained. The invisibility of the iron oxide nanoparticles in TEM can be explained if part of the extracted and dissolved silicon precipitates onto the surface of the zeolite crystals, as reported previously [34,35]. The dissolved siliceous species may form a layer of amorphous silica covering the iron oxide. If so, the layer should be sufficiently thin to achieve a very similar electrochemical response during voltammetric characterization of the alkaline-treated and steamed zeolites.

Gang et al. [39] have recently reported the improved activity of Cu–Y zeolite for ammonia oxidation to N_2 after an NaOH treatment, according to the procedure reported by Suzuki et al. [40]. This was attributed to a change in the constitution of the catalyst with respect to copper, by formation of copper–oxygen aggregates, $[Cu–O–Cu]^{2+}$, inside the zeolite supercage. However, no experimental evidence was provided to support this statement. In our systems, the nature of the iron sites before and after alkaline treatment appear quite similar based on the voltammetric response, although, as previously stated, quantification is not possible. A lower onset temperature for N_2O decomposition is also not expected if more active sites are created, since the oxygen desorption is the rate-determining step. Nevertheless, the improved activity of *ex*-[Fe,Al]MFI(*at*) is most likely explained by an improved accessibility as a consequence of mesopore creation. The catalyst with small crystals may also

already suffer from diffusion limitations at higher temperatures.

From the results along the manuscript the intrazeolitic nature of the active iron species in direct N_2O decomposition and the minor role of extrazeolitic iron oxide particles seems to be clear. As discussed elsewhere [41], oligonuclear species are preferred over isolated ions in view of the easier oxygen recombination (rate-determining step in direct N_2O decomposition) of two iron centers that are close together. However, the number of iron atoms in an active cluster cannot be assessed from our current results. In view of the heterogeneous nature of the FeMFI system, it would be of no surprise to have a distribution of active oligonuclear centers. A conclusive answer may be obtained from the synthesis of FeMFI zeolites with uniform iron species, a challenging task.

5. Conclusions

The following conclusions can be derived from this study:

- Extra-framework iron species generated during steam treatment play an essential role in direct catalytic N_2O decomposition. Framework iron is unable to activate N_2O and thus is inactive in the reaction. Extra-framework Al and Ga species (Lewis acidic centers) and Brønsted acidic sites also play a minor role.
- The dislodgment of framework iron leads to a variety of iron species. The catalyst constitution, i.e., the nature and relative amounts of the various iron species in the catalyst, is greatly affected by the conditions of the steam treatment (temperature and partial steam pressure). An optimum in temperature is found, to achieve the extraction of inactive framework iron but to avoid extensive clustering into inactive iron oxide particles. Activation under steam-rich conditions reduces the temperature for a certain iron extraction and induces a more tender clustering.
- Electrochemical characterization can be used to identify framework and different extraframework iron species upon steaming under different conditions and to visualize the clustering process, i.e., whether too harsh or too mild steaming conditions have been used. However, no quantification of relative amounts of various iron species is possible due to the intrinsic nature of the technique (surface-mediated electron-transfer mechanism).
- The optimal activation conditions depend on the composition of the zeolite framework. The presence of Al or Ga provides an easier escape route of iron to extra-framework positions and significantly reduces the activation temperature for maximal N_2O conversion (873–923 K) compared to Fe-silicalite (1123 K).
- The intrazeolitic nature of the iron species in direct N_2O decomposition over FeMFI zeolites is supported by the presence of measurable intracrystalline diffusion limitations in catalysts with larger crystal size. Alkaline treatment of the steamed zeolite leads to improved N_2O decomposition activities, a consequence of the largely improved accessibility and gas transport by mesopore formation. This aspect is considered a key design factor for an optimized FeMFI catalyst in various processes.

Acknowledgment

Dr. P.J. Kooyman is gratefully acknowledged for performing the TEM experiments.

References

[1] G.I. Panov, CATTECH 4 (2000) 18.
[2] A. Ribera, I.W.C.E. Arends, S. de Vries, J. Pérez-Ramírez, R.A. Sheldon, J. Catal. 195 (2000) 287.
[3] A.S. Kharitonov, G.I. Panov, G.A. Sheveleva, L.V. Pirutko, T.P. Voskresenskaya, V.I. Sobolev, US Patient 5,672,777, 1997, assigned to Solutia.
[4] P. Notté, Top. Catal. 13 (2000) 387.
[5] L.V. Pirutko, V.S. Chernyavsky, A.K. Uriarte, G.I. Panov, Appl. Catal. A 227 (2002) 143.
[6] J. Pérez-Ramírez, F. Kapteijn, G. Mul, J.A. Moulijn, Chem. Commun. (2001) 693.
[7] J. Pérez-Ramírez, F. Kapteijn, G. Mul, J.A. Moulijn, Appl. Catal. B 35 (2002) 227.
[8] J. Pérez-Ramírez, G. Mul, F. Kapteijn, J.A. Moulijn, A.R. Overweg, A. Doménech, A. Ribera, I.W.C.E. Arends, J. Catal. 207 (2002) 113.
[9] K.A. Dubkov, N.S. Ovanesyan, A.A. Shteinman, E.V. Stakoron, G.I. Panov, J. Catal. 207 (2002) 341.
[10] A.M. Ferretti, C. Oliva, L. Forni, G. Berlier, A. Zecchina, C. Lamberti, J. Catal. 208 (2002) 83.
[11] J.C. Groen, J. Pérez-Ramírez, L.A.A. Peffer, Chem. Lett. (2002) 94.
[12] B.C. Lippens, J. de Boer, J. Catal. 4 (1965) 319.
[13] E.P. Barret, L.G. Joyner, P.H. Halenda, J. Amer. Chem. Soc. 73 (1951) 373.
[14] A. Doménech, J. Pérez-Ramírez, A. Ribera, F. Kapteijn, G. Mul, J.A. Moulijn, Catal. Lett. 78 (2002) 303.
[15] J. Pérez-Ramírez, R.J. Berger, G. Mul, F. Kapteijn, J.A. Moulijn, Catal. Today 60 (2000) 93.
[16] A.V. McCormick, A.T. Bell, Catal. Rev. Sci. Eng. 31 (1989) 97.
[17] J.C. Jansen, in: H. van Bekkum, E.M. Flanigen, J.C. Jansen (Eds.), Introduction to Zeolite Science and Practice, Elsevier, Amsterdam, 1991.
[18] C.R. Bayense, A.P.M. Kentgens, J.W. de Haan, L.J. van de Ven, J.H.C. van Hooff, J. Phys. Chem. 96 (1992) 775.
[19] C.R. Bayense, J.H.C. van Hooff, A.P.M. Kentgens, J.W. de Haan, L.J. van de Ven, J. Chem. Soc. Chem. Commun. (1989) 1292.
[20] R.A. Le Febre, High-silica zeolites and their use as catalyst in organic chemistry, PhD thesis, Delft University of Technology, 1989.
[21] M. Ogura, S. Shinomiya, J. Tateno, Y. Nara, M. Nomura, E. Kikuchi, M. Matsukata, Appl. Catal. A 219 (2001) 33.
[22] A. Doménech, J. Pérez-Ramírez, G. Mul, F. Kapteijn, I.W.C.E. Arends, J. Electroanal. Chem. 519 (2002) 72.
[23] G. Mul, J. Pérez-Ramírez, F. Kapteijn, J.A. Moulijn, Catal. Lett. 80 (2002) 129.
[24] L.V. Pirutko, O.O. Parenago, E.V. Lunina, A.S. Kharitonov, L.G. Okkel, G.I. Panov, React. Kinet. Catal. Lett. 52 (1994) 275.
[25] G.I. Panov, A.S. Kharitonov, V.B. Fenelonov, T.P. Voskresenskaya, N.A. Rudina, V.V. Molchanov, L.M. Plyasova, Zeolites 15 (1995) 253.

[26] J. Pérez-Ramírez, F. Kapteijn, G. Mul, J.A. Moulijn, Catal. Commun. 3 (2002) 19.
[27] G. Spoto, A. Zecchina, G. Berlier, S. Bordiga, M.G. Clerici, L. Basini, J. Mol. Catal. A Chem. 158 (2000) 107.
[28] A.S. Kharitonov, G.A. Sheveleva, G.I. Panov, V.I. Sobolev, Y.A. Paukshtis, V.N. Romannikov, Appl. Catal. A 98 (1993) 33.
[29] G.I. Panov, V.I. Sobolev, A.S. Kharitonov, in: S. Yoshida, N. Takazawa, T. Ono (Eds.), Catalysis Science and Technology, Vol. 1, Kodansha, Tokyo, 1991, p. 171.
[30] T. Tabata, H. Ohtsuka, Catal. Lett. 48 (1997) 203.
[31] A. Sichi, A. Satsuma, M. Iwase, K. Shimizu, S. Komai, T. Hattori, Appl. Catal. B 17 (1998) 107.
[32] R.M. Barrer, M.B. Makki, Can. J. Chem. (1964) 42.
[33] R.M. Dessau, E.W. Valyocsik, N.H. Goeke, Zeolites 12 (1992) 776.
[34] R.L.V. Mao, S. Xiao, A. Ramsaran, J. Yao, J. Mater. Chem. 4 (1994) 605.
[35] C.S. Cundi, M.S. Henty, R.J. Plaisted, Zeolites 15 (1995) 342.
[36] A. Cizmek, B. Subotic, R. Aiello, F. Crea, A. Nastro, C. Tuoto, Micropor. Mater. 4 (1995) 159.
[37] A. Cizmek, B. Subotic, I. Smit, A. Tonejc, R. Aiello, F. Crea, Micropor. Mater. 8 (1997) 159.
[38] M. Ogura, S. Shinomiya, J. Tateno, Y. Nara, E. Kikuchi, M. Matsukata, Chem. Lett. (2000) 882.
[39] L. Gang, J. van Grondelle, B.G. Anderson, R.A. van Santen, J. Catal. 186 (1999) 100.
[40] M. Suzuki, K. Tsutsumi, H. Takahashi, Y. Saito, Zeolites 8 (1988) 387.
[41] J. Pérez-Ramírez, F. Kapteijn, G. Mul, J.A. Moulijn, J. Catal. 208 (2002) 211.